Title

PARP7 Inhibitors and AHR Agonists Act Synergistically Across a Wide-Range of Cancer Models.

Authors

Chen, Huadong
Gou, Xuxu
Mao, Ying
et al.

Publication Date

2024-09-24

DOI

10.1158/1535-7163.mct-24-0211

Peer reviewed

PARP7 Inhibitors and AHR Agonists Act Synergistically across a Wide Range of Cancer Models

Huadong Chen, Xuxu Gou, Ying Mao, Patrick C. O'Leary, Morgan E. Diolaiti, and Alan Ashworth

ABSTRACT

Small-molecule inhibitors of the mono (ADP) ribosyl transferase PARP7 are being evaluated asmonotherapy for tumors overexpressing PARP7 and in combination with immune checkpoint blockade. We previously showed that sensitivity to the PARP7 inhibitor (PARP7i) RBN-2397 could be enhanced by cotreatment with agonists of the aryl hydrocarbon receptor (AHRa) in cell lines that show strong intrinsic sensitivity to RBN-2397. In this study, we demonstrated that a range of tumor cell lines that are relatively insensitive to PARP7i or AHRa as individual agents are unexpectedly profoundly sensitive to their combination. Our data show that this synergistic response is dependent on the AHR/AHR nuclear translocator and is associated with increased levels of nuclear AHR and increased transcription of AHR target genes. In some hormone receptor–positive cell lines, we find that combination treatment is associated with proteasomal turnover of the steroid hormone receptors, androgen receptor and estrogen receptor. Both wild-type and hormone-resistant mutant forms of these receptors are degraded upon treatment with AHRa and PARP7i in breast and prostate cancer models. These results suggest that combining PARP7i with AHRa may extend the utility of these drugs to a wider range of tumors, including those that are refractory to hormone therapy.

Introduction

The aryl hydrocarbon receptor (AHR) is a ligand-activated helix-loop-helix transcription factor that plays an important role in maintaining cellular homeostasis, differentiation, and immunity (1). The AHR was originally described as a sensor of xenobiotic chemicals that regulates biological responses to planar aromatic hydrocarbons, including 2,3,7,8-tetrachlorodibenzo-p-dioxin (dioxin). More recently, potential endogenous ligands of the AHR, including kynurenine, have been described (2–4). Upon ligand binding, the AHR translocates from the cytoplasm into the nucleus, in which, as a dimer with the AHR nuclear translocator (ARNT), it promotes transcription of multiple genes, including the drug metabolism enzymes cytochromes P450 (CYP) *CYP1A1*, *CYP1A2*, *CYP1B1*, and UDP glucuronosyltransferase 1 family polypeptide A6 (*UGT1A6*) and other genes such as the 2,3,7,8-tetrachlorodibenzo-p-dioxin–inducible mono (ADP) ribosyl transferase *TiPARP*, also known as *PARP7*.

The regulation of AHR activation is a dynamic process. Concurrent with AHR-mediated transcription, AHR begins to be exported from the nucleus to the cytoplasm, in which it is subjected to proteasomal degradation. The AHR is a target of PARP7-mediated ADP-ribosylation (5), and we and other researchers have shown that PARP7 activity is important for nuclear export of the AHR and that loss of PARP7 activity leads to an accumulation of nuclear AHR (6). In the nucleus, the ligand-bound AHR can become associated with an atypical E3 ligase complex containing Cullin4B (CUL4B), RBX1, TBL3, and DDB1 (7), and among the substrates of this $CUL4B^{AHR}$ complex are steroid receptors, including estrogen receptor α (ERα), ERβ, and the androgen receptor (AR; ref. 8).

Most breast cancers express ERα and are fueled by estrogen and ER signaling (9). In the nucleus of ERα-positive cells, estrogen-bound ERα dimerizes and binds to estrogen response elements within ER canonical genes, recruiting transcriptional coactivators to initiate gene expression and drive cell proliferation (9). Endocrine therapies (ET) that block estrogen production or inhibit ER function are standard-of-care treatments for ERα-positive breast cancer, including aromatase inhibitors, selective ER modulators (e.g., tamoxifen), and selective ER degraders (e.g., fulvestrant) that bind the ligand-binding domain of the ER, prevent receptor dimerization and induce degradation of the ER (10). Despite the efficacy of ET, some patients eventually acquire drug resistance and develop lethal metastasis after an initial response. One well-established mechanism of ET resistance is the emergence of point mutations in the ligand-binding domain of *ESR1* (the gene encoding ERα), identified in up to 40% of metastatic ERα-positive breast cancers (11–13); these mutations drive constitutive ET-resistant activation of ER target genes (12–14). AR-positive prostate cancer is also driven by sex hormones. Various *AR* mutations, including variant 7 (v7), have been demonstrated to render antiandrogen resistance and metastasis, and metastatic castration-resistant prostate cancer is almost invariably fatal. FDA-approved therapies for metastatic castration-resistant prostate cancer extend patient survival for an average of only a few months (15, 16), and therefore, there is an urgent need to develop new effective therapeutic approaches.

PARP7 has emerged as a potential therapeutic target for cancer, in part because some breast cancers have elevated expression levels of *PARP7* mRNA (17). RBN-2397, a specific and selective PARP7 inhibitor (PARP7i), has been shown to have both cell autonomous and nonautonomous effects (8, 18, 19); this first-in-class inhibitor is currently being evaluated as a monotherapy and in combination with immune checkpoint blockade to treat solid tumors (NCT04053673 and NCT05127590). The rationale for these combination trials is that inhibition of PARP7 may restore type I IFN

Helen Diller Family Comprehensive Cancer Center, University of California, San Francisco, San Francisco, California.

H. Chen and X. Gou contributed equally to this article.

Corresponding Author: Alan Ashworth, Helen Diller Family Comprehensive Cancer Center, UCSF, 1450 3rd Street, Room HD-271, Box 0128, San Francisco, CA 94158. E-mail: Alan.Ashworth@ucsf.edu

Mol Cancer Ther 2024;XX:XX–XX

doi: 10.1158/1535-7163.MCT-24-0211

signaling responses in tumor models, thus blocking pathways that cancer cells use to evade immune detection (18–21).

We previously described a genome-wide CRISPR/Cas9 loss-of-function screen to identify determinants of sensitivity to the PARP7i RBN-2397 (22). This study revealed that inactivation of the *AHR* gene rendered the PARP7i-sensitive cell line NCI-H1373 resistant to the drug. In contrast, an AHR agonist (AHRa) enhanced the sensitivity of NCI-H1373 and other RBN-2397-sensitive cells to PARP7i. In the current study, we tested the effect of combining PARP7i and AHRa across a panel of cell lines. Our results reveal that PARP7i and AHRa can induce a synergistic lethal effect in cells that are insensitive to either single agent. Amongst these cell lines, breast and prostate cell models that are resistant to estrogen or androgen blockade therapies are responsive to the combination of PARP7i and AHRa, suggesting that targeting the PARP7/AHR axis may be a novel therapeutic strategy to treat hormone refractory tumors.

Materials and Methods

Cell culture

Human K562, HCC1395, HGC27, NCI-N87, SW48, HCC1937, BT474, 22Rv1, LNCaP, C4-2, C4-2B, PC-3, COV362, PEO1, PEO4 JHOS-2, OVCAR3, DLD1, A375, NCI-H1437, HEK293T, MDA-MB-436, U2OS, HCT116, MDA-MB-468 (HTB-132), MDA-MB-231, MCF-7, T-47D, MDA-MB-157, A549, NCI-H1299, SW620 (CCL-227), CAL27, HT-29, SK-BR-3, MCF10A, AGS, UWB1.289, LAPC4, and Capan-1 cells were obtained from the ATCC. Human HAP1 (C631) cells were purchased from Horizon Discovery. $CD8^+$T cells were enriched from TRIMA Residual ordered from Blood Centers of the Pacific using EasySep Human $CD8^+$ T Cell Isolation Kit, Cat. # 17953) and grown in complete *X-vivo* media with +5% FBS, 10 mmol/L N-acetyl cysteine, 55 μmol/L β-mercaptoethanol, and 50 IU/mL IL2. K562, HCC1395, HGC27, NCI-N87, SW48, HCC1937, BT474, T-47D, 22Rv1, LnCaP, C4-2, C4-2B, PC-3, COV362, PEO1, PEO4, JHOS-2, OVCAR3, DLD1, A375, and NCI-H1437 cells were grown in RPMI 1640 Medium (ATCC modification) with 10% FBS and 1% penicillin–streptomycin. HEK293T, MDA-MB-436, U2OS, HCT116, MDA-MB-468, MDA-MB-231, MCF-7, MDA-MB-157, A549, NCI-H1299, SW620, and CAL27 cells were grown in DMEM with 10% FBS and 1% penicillin–streptomycin. HT-29 and SK-BR-3 cells were grown in McCoy's 5A (modified) with 10% FBS and 1% penicillin–streptomycin. MCF10A cells were grown in DMEM/F12 with 5% horse serum, 20 ng/mL EGF, 0.5 mg/mL hydrocortisone, 100 ng/mL cholera toxin, 10 μg/mL insulin, and 1% penicillin–streptomycin. AGS, UWB1.289, and Hela cells were grown in DMEM/F12 with 10% FBS and 1% penicillin–streptomycin. HAP-1, LAPC4, and Capan-1 cells were grown in Iscove's Modified Dulbecco's Medium with 10% FBS and 1% penicillin–streptomycin. MCF-7 cells expressing HER2 L755S were gifts from Dr. Ben Ho Park at Vanderbilt University and Dr. Shyam M. Kavuri at Baylor College of Medicine. MCF-7, 22Rv1, and C4-2 cells were authenticated by short tandem repeat profiling and tested for *Mycoplasma* at Labcorp.

Drug response assay

Short-term survival assays were performed as previously described. In brief, cells were seeded into 96-well plates at a concentration of 1,000 cells per well. The next day, cells were treated with RBN-2397 (MedChemExpress, HY-136174; PubChem CID: 146047148), tapinarof (Selleck Chemicals, S9700; PubChem CID: 6439522), 10-CI-BBQ (Tocris Bioscience, 63-215; PubChem CID: 1778614), and 6-formylindolo(3,2-b) carbazole (FICZ; MedChemExpress, HY-12451; PubChem CID: 1863) at the indicated concentrations. After 7 days, cell viability was assessed by CellTiter-Glo assay (Promega, G7572) or confluency and/or cell number (Nuclight-RFP) were assessed by IncuCyte Live-Cell Analysis System (Sartorius).

RNA sequencing and gene set enrichment analysis

22Rv1 cells were hormone-deprived in charcoal-stripped serum-containing phenol red–free RPMI media (CSS media) for 3 days and treated with vehicle, 5 nmol/L DHT + DMSO, 5 nmol/L DHT + 100 nmol/L RBN-2397, 5 nmol/L DHT + 100 nmol/L tapinarof, or 5 nmol/L DHT + 100 nmol/L RBN-2397 + 100 nmol/L tapinarof for 48 hours. The experiment was conducted in biological duplicates. RNA was isolated using RNeasy Mini Kit (QIAGEN, 74104) and treated with DNase (QIAGEN, 79254) to remove genomic DNA. Library preparation (Agilent RNA 6000 Nano Kit) and strand-specific sequencing (30 mol/L reads, PE150) was performed by BGI using a DNBSEQ platform. Fastq files, BAM files, and differential gene expression data were generated by BGI (https://www.bgi.com/us/home). For RNA sequencing (RNA-seq) analysis, reads were aligned to the hg38 (GRCh38) reference genome using Bowtie2 (23). Gene expression levels for each sample were calculated as transcripts per million using RSEM (24). Gene set enrichment analysis (GSEA) was performed using WebGestalt (RRID: SCR_006786; ref. 25). WikiPathway enrichment bubbles were plotted using SRplot (http://www.bioinformatics.com.cn/srplot).

Construction of plasmids

The primers used for the construction of plasmids are listed in Supplementary Table S1. All plasmids were verified by Sanger sequencing. To construct the PB-TRE-Myc-DDK-PARP7 plasmid, we PCR-amplified a *PARP7* fragment from the *TiPARP* cDNA (OriGene, RC230398) and used a Gibson cloning kit (New England Biolabs E5510) to clone these fragments into a Nhe1/Pme1-digested PB-Tre backbone (Addgene plasmid, #63800). To construct the PB-TRE-Myc-DDK-AHR plasmid, a Myc-DDK–tagged AHR fragment was PCR-amplified from the *AHR* (Myc-DDK–tagged) plasmid (OriGene, RC209832) and Gibson cloning was used to clone this fragment into the Nhe1/Pme1-digested PB-TRE backbone (Addgene plasmid, #63800). The lentiCRISPRv2 single-guide RNA (sgRNA) plasmids were constructed using the method previously described by the Zhang Lab and the sgRNA oligos in Supplementary Table S2. A detailed protocol is available at https://media.addgene.org/cms/filer_public/4f/ab/4fabc269-56e2-4ba5-92bd-09dc89c1e862/zhang_lenticrisprv2_and_lentiguide_oligo_cloning_protocol_1.pdf. PB-TRE-dCas9-VPR was a gift from George Church (Addgene plasmid, #63800; http://n2t.net/addgene:63800; RRID: Addgene_63800).

Lentiviral packaging

Lentivirus was prepared as previously described (26). Briefly, 15 million HEK293T cells were grown overnight on 15-cm poly-L-lysine–coated dishes and then transfected with 6 μg pMD2.G (Addgene plasmid, #12259; http://n2t.net/addgene:12259; RRID: Addgene_12259), 18 μg dR8.91 (since replaced by second-generation compatible pCMV-dR8.2, Addgene plasmid, #8455, RRID: Addgene_8455), and 24 μg lentiCRISPRv2 sgRNA plasmids or pBOB-EF1-FastFUCCI-Puro (Addgene plasmid, # 86849; http://n2t.net/addgene:86849; RRID:

Addgene_86849) using the Lipofectamine 3000 transfection reagent as per the manufacturer's protocol (Thermo Fisher Scientific, Cat. # L3000001). pMD2.G and dR8.91 were a gift from Didier Trono. pBOB-EF1-FastFUCCI-Puro was a gift from Kevin Brindle and Duncan Jodrell. The following day, media was refreshed, and viral boost reagent was added at 500× as per the manufacturer's protocol (Alstem, Cat. #VB100). The viral supernatant was collected 48 hours after transfection and spun down at 300 *g* for 10 minutes to remove cell debris. To concentrate the lentiviral particles, Alstem precipitation solution (Alstem, Cat. #VC100) was added, mixed, and refrigerated at 4°C overnight. The virus was then concentrated by centrifugation at 1,500 *g* for 30 minutes at 4°C. Finally, each lentiviral pellet was resuspended in 100× of original volume in cold DMEM + 10% FBS + 1% penicillin–streptomycin and stored at −80°C.

Establishment of individual CRISPR knockout cells

To generate knockout (KO) clones for individual genes, MCF-7, MCF-7 *ESR1*-mutant, and 22Rv1 cells were transduced with lentiV2 plasmids containing sgRNAs of hit genes or a nontargeting sgRNA (sgNC). Infected cells were selected for 3 days with 2 μg/mL puromycin and single cell–cloned by limiting dilution. Individual clones were screened and validated by western blotting and/or qRT-PCR.

Western blotting

Cell lysates were prepared in Pierce RIPA Buffer (Thermo Fisher Scientific, 89901) containing protease inhibitor and PhosStop cocktails (Roche, 5892970001 and 4906845001) separated on SDS-PAGE and transferred to a polyvinylidene difluoride membrane. The following antibodies were used for immunoblotting: anti-AHR [Cell Signaling Technology (CST), 83200S, RRID: AB_2800011]; anti–β-actin [horseradish peroxidase (HRP) conjugate; CST, 5125S, RRID: AB_1903890]; anti–Myc-Tag (CST, 2040S); anti–poly/mono-ADP ribose (CST, 83732S, RRID: AB_2749858); anti–hypoxia-inducible factor-1β/ARNT (CST, 5537S, RRID: AB_10694232); anti-ubiquitin (Novus Biologicals, NB300129, RRID: AB_2180546); anti–topoisomerase I (Abcam, ab109374, RRID: AB_10861978); anti–phospho-Rb (Ser807/811; CST, 8516, RRID: AB_11178658); anti-Rb (CST, 9309, RRID: AB_823629); anti-p21 (CST, 2947, RRID: AB_823586); anti–PARP-1 (Santa Cruz Biotechnologies, sc-8007, RRID: AB_628105); anti-ERα (Millipore Sigma, 04-820, RRID: AB_1587018); anti-AR (CST, 5153, RRID: AB_10691711), GAPDH (CST, 3683, RRID: AB_1642205); anti-rabbit HRP antibody (CST, 7074P2, RRID: AB_2099233), and anti-mouse HRP antibody (CST, 7076S, RRID: AB_330924). Membranes were developed using ECL reagent (ProSignal Femto, Cat. # 20-302B).

qRT-PCR

Total RNA was isolated using RNeasy Mini Kit (Qiagen, 74104), and 500 ng of total RNA was used to prepare cDNA using PrimeScript RT Master Mix (TAKARA, RR036A) according to the manufacturer's instructions. qRT-PCR was performed in triplicates for each target sequence using iTaq Universal SYBR Green Supermix (Bio-Rad, 1725121) on Bio-Rad CFX96 using the primers in Supplementary Table S3. Cells were treated with 1 μmol/L RBN-2397, tapinarof, and/or 10-CI-BBQ. This dose was selected as the dose at which each individual drug had minimal effects on cell viability.

PiggyBac AHR/PARP7 induced expression cell construction

MCF-7 and 22Rv1 were cotransfected with the PiggyBac transposase vector (System Bioscience, NC1271867) and PB-TRE-Myc-DDK-AHR or PB-TRE-Myc-DDK-PARP7. The next day, the medium was changed, and cells were cultured for additional 48 hours before being selected with hygromycin (20 μg/mL) for 5 to 7 days. During selection, media containing fresh hygromycin was replaced every 2 days. After selection, cells were expanded, and AHR expression was induced with 1 μg/mL doxycycline for 48 hours and confirmed by western blotting. To measure the effect of AHR expression on cell proliferation, cells were seeded into 96-well plates. Twenty four hours later, AHR expression was induced by doxycycline (1 μg/mL), and cell proliferation (cell confluence) was measured using the IncuCyte ZOOM Live-Cell Analysis System (Sartorius).

Nuclear and cytoplasmic protein extraction

Two million MCF-7 and 22Rv1 cells were seeded in 6-well plates. The next day, cells were treated with RBN-2397 (MedChemExpress, HY-136174) and/or tapinarof (Selleck Chemicals, S9700) at the indicated concentrations for 4 hours. Nuclear and cytoplasmic extraction using NE-PER nuclear and cytoplasmic extraction reagents according to the manufacturer's instructions (Thermo Fisher Scientific, 78833).

Quantitative FastFUCCI assay

Two million MCF-7, MCF-7 *ESR1* Y537S, 22Rv1, and C4-2 cells were seeded in 10-cm dishes and transduced with pBOB-EF1-FastFUCCI-Puro *Lentivirus* in the presence of 8 μg/mL polybrene. After 24 hours, the media was changed, and after 48 hours, fresh medium containing 1 μg/mL puromycin was added to select infected cells. Cells were selected for 72 hours and then expanded. Red fluorescent cells (i.e., cells in G1) were enriched by flow cytometry using a FACSAria 3 cell sorter (BD Biosciences). FastFUCCI-expressing cells were seeded into 96-well plates and treated with the indicated concentrations of RBN-2397 and/or tapinarof. After 48 to 72 hours, fluorescent cells were scanned using the IN-Cell Analyzer 6500 System and then analyzed by IN Cell Developer (Cytiva).

AHR subcellular distribution assay

To assess endogenous AHR and exogenous PARP7 localization, MCF-7, MCF-7 *PARP7* KO, and MCF-7 *PARP7* KO PB-TRE-PARP7 cells that endogenously expressed AHR proteins were seeded in 96-well plates (5,000 cells/well). MCF-7 *PARP7* KO PB-TRE-PARP7 cells were pre-treated with 1 μg/mL doxycycline for 24 hours to induce the expression of PARP7. These three cell lines were then treated the next day with the indicated concentrations of RBN-2397 and/or tapinarof. After 2 hours of exposure to drugs, treated cells were fixed in precooled methanol at −20°C for 20 minutes, blocked in 3% BSA for 15 minutes, incubated with anti–AHR-rabbit (CST, 83200S) or anti–Myc-Tag-mouse (CST, 2276S) antibodies for 1 hour, and then incubated with goat anti-rabbit IgG secondary antibody, Alexa Fluor 488 (Thermo Fisher, A-11008) and goat anti-mouse IgG secondary antibody, Alexa Fluor 555 (Thermo Fisher, A-32727) secondary antibodies for 30 minutes and stained with DAPI (4',6-diamidino-2-phenylindole) for 10 minutes. Fluorescent cells were imaged using the IN Cell Analyzer 6500 System (Cytiva) and analyzed using IN Carta software (Cytiva).

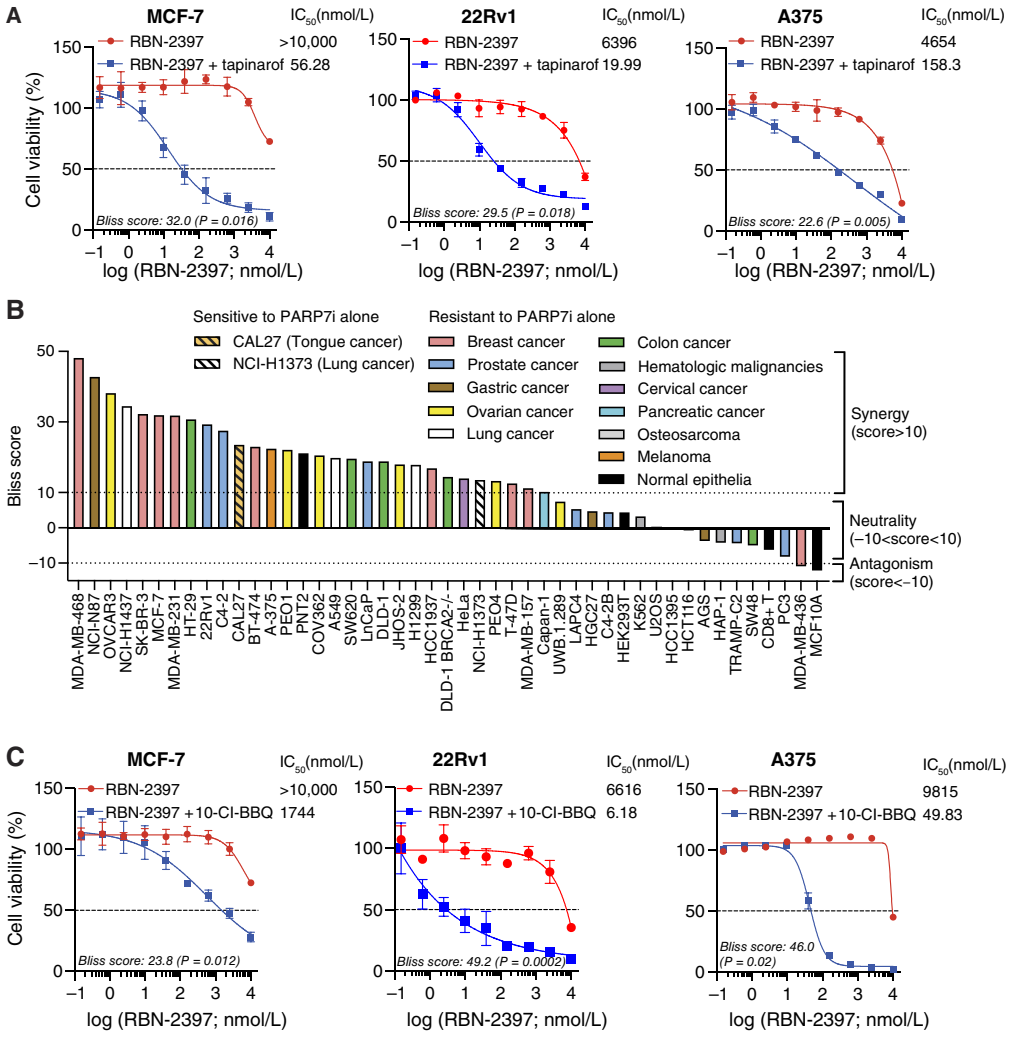

Figure 1.

AHRa and PARP7a are synergistically lethal. **A,** Survival curves (CellTiter-Glo) of MCF-7, 22Rv1, and A375 cancer cells exposed to increasing concentrations of RBN-2397 with or without a fixed concentration of tapinarof (100 nmol/L). **B,** Bliss synergy scores of RBN-2397 with a fixed tapinarof concentration (100 nmol/L) in 47 cell lines. Scores are represented as synergy (score > 10), neutrality (score −10 to +10), or antagonism (score < −10). **C,** Survival curves (CellTiter-Glo) of MCF-7, 22Rv1, and A375 cancer cells exposed to increasing concentrations of RBN-2397 with or without a fixed concentration of 10-Cl-BBQ (100 nmol/L). All data are plotted as the mean ± SD; $n = 3$. Bliss scores with P values are indicated.

Generation of *ESR1*-mutant cell lines

MCF-7 *ESR1*-mutant cell lines were generated by CRISPR-Cas9 editing. MCF-7 cells were transfected with a Cas9 expression plasmid containing *ESR1*-targeting sgRNA (5′-CCGCCTACATGCGCCCAC-TA-3′) and single-stranded oligonucleotide donor templates. Cells were subject to fluorescence-activated cell sorting and plated into 96-well plates (1 cell/well). Individual clones were expanded for genomic DNA extraction and PCR amplification of genomic DNA. Successful knock-in of each mutation was confirmed by Sanger sequencing of the PCR products. Total DNA was isolated from MCF-7 wild-type (WT) and *ESR1*-mutant expressing cell lines using DNeasy Blood & Tissue Kits (Qiagen, Cat. # 69504). A measure of 500 ng of total DNA was used to amplify the sequences of *ESR1* WT, Y537S, Y537C, and D538G using TaKaRa Ex Taq (TaKaRa, RR001A) on Eppendorf Mastercycler X50s using primers 5′-AGGGATTTCAGCACTCCTGG-3′ and 5′-CGT-GATGTAATACTTTTGCAAGG-3′. The PCR products were further characterized and validated by DNA sequencing (MCLAB).

RNA interference

siRNA knockdown experiments were conducted using Lipofectamine 3000 Transfection Reagent (Invitrogen, L3000075) according to the manufacturer's protocol. A measure of 100 nmol/L Dharmacon nontargeting control siRNA or human *AR* siRNA (Invitrogen, s1539) was used. Knockdown cells were assayed for cell viability 48 hours after transfection.

Data analysis

All data, if applicable, are presented as the mean ± SD. Significant differences were determined by the Student t test. $P < 0.05$ was considered statistically significant. Dose curves and bar graphs were

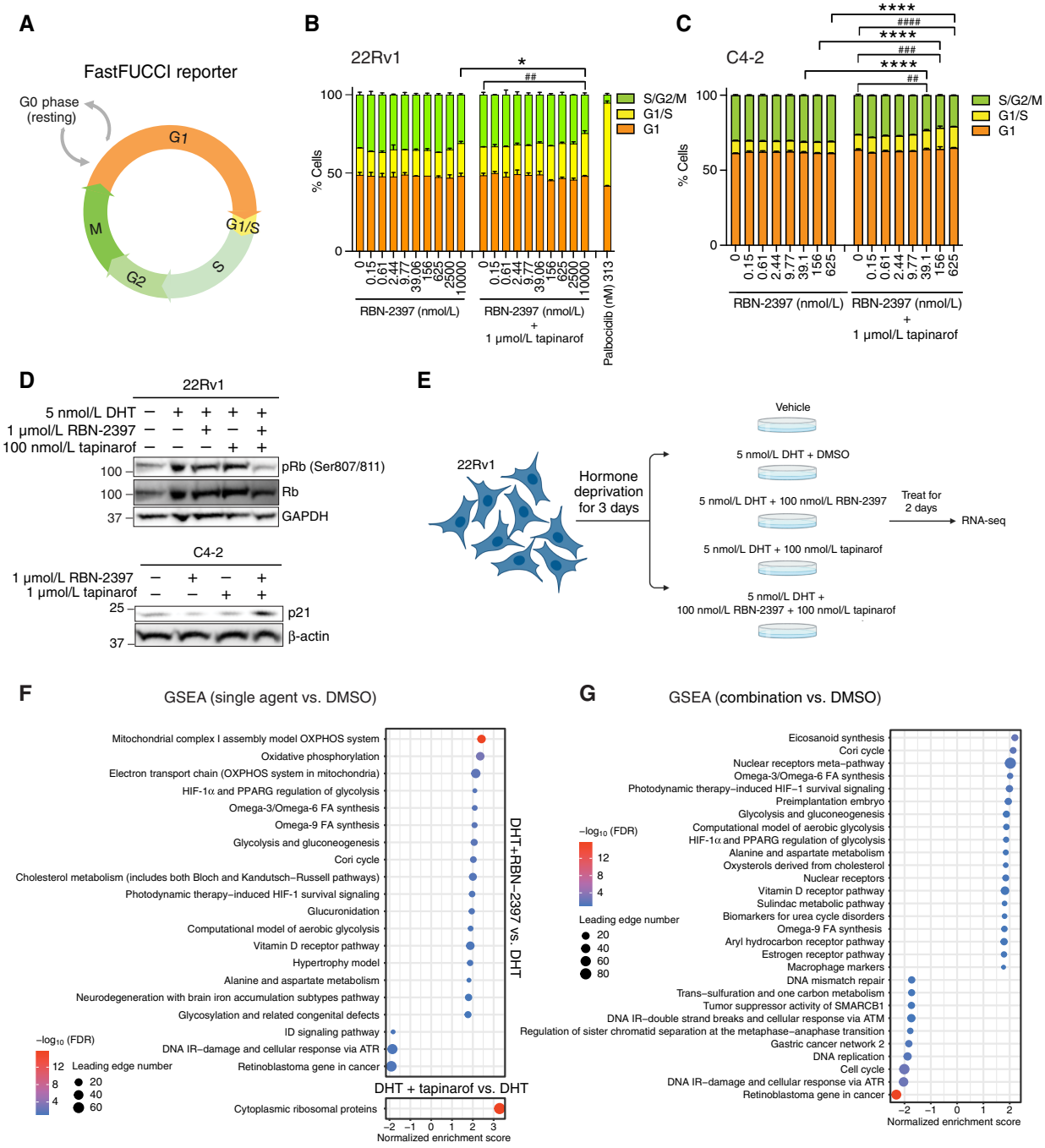

Figure 2.

PARP7i and AHRa induce cell-cycle arrest and alter transcriptional profiles. **A,** Schema of the FastFUCCI reporter. **B** and **C,** Plots showing the percent of 22Rv1 (**B**) and C4-2 (**C**) cells in each phase of the cell cycle after treatment with indicated concentrations of RBN-2397 and tapinarof for 72 hours. Green, yellow, and orange correspond to S/G2/M, G1/S, and G1, respectively. One-way ANOVA followed by Tukey multiple comparisons test was used to compare the fraction of cells in S/G2/M for each treatment. */#, $P < 0.05$; **/##, $P < 0.01$; ***/###, $P < 0.001$; ****/####, $P < 0.0001$. 22Rv1 cells treated with palbociclib are shown as a positive control. **D,** Western blot analysis of lysates from 22Rv1 and C4-2 cells treated with the indicated combinations of RBN-2397 and/or tapinarof for 48 hours. **E,** Workflow of RNA-seq on 22Rv1 cells. **F** and **G,** Bubble plots showing pairwise GSEA of differentially regulated WikiPathways after indicated treatments. (**A** and **E**, Created with BioRender.com). HIF, hypoxia-inducible factor.

generated using GraphPad Prism 9 (RRID: SCR_002798). To generate survival curves, raw cell viability data were normalized to the DMSO control wells, and drug concentrations on the *x*-axis were $\log_{10}$-transformed. Synergy was quantified by Bliss score using SynergyFinder (27). The workflow of RNA-seq was created using BioRender (RRID: SCR_018361).

Data availability

The data generated in this study are available within the article and its supplementary data files. Gene expression data can be obtained from the NCBI Gene Expression Omnibus (GEO) database with accession number: GSE269640.

Results

Testing the effects of PARP7i and AHRa

To further explore the relationship between PARP7 and the AHR, we tested the response of a range of cell lines to PARP7i and AHRa either as single agents or in combination. Unexpectedly, we discovered that many tumor cell lines that are relatively insensitive to RBN-2397 (a PARP7i) or tapinarof (an AHRa) alone were profoundly sensitive to the combination of these agents. Compared with RBN-2397 alone, the addition of 100 nmol/L tapinarof significantly shifted the IC_{50} values in multiple breast, prostate, ovarian, lung, colon, gastric, cervical, pancreatic, and melanoma cancer cell lines, with the majority of cancer cell lines having Bliss synergy scores >10 (**Fig. 1A** and **B**; Supplementary Fig. S1A). A measure of 100 nmol/L tapinarof was selected for this experiment because this concentration was shown to not affect cell proliferation (Supplementary Fig. S1D). This synergistic effect was largely absent in nontransformed cell lines, primary T cells, and in some cancer models (**Fig. 1B**; Supplementary Fig. S1A and S1B) and was not specific to tapinarof, as other AHRa, including 10-CI-BBQ and FICZ, also showed synergy with RBN-2397 (**Fig. 1C**; Supplementary Fig. S1C). Complementary experiments in which the RBN-2397 concentration was held constant and the dose of AHRa (tapinarof or 10-CI-BBQ) was varied showed a similar effect (Supplementary Fig. S1D and S1E). The above results demonstrate that the combination of AHRa and PARP7i can selectively inhibit the growth of many tumor cell lines, including many that were insensitive to PARP7i, potentially expanding the therapeutic utility of PARP7i.

The combination of PARP7i and AHRa induces cell-cycle arrest and alters transcriptional profiles

To explore how the combination of PARP7i and AHRa affects cell growth, we engineered 22Rv1, C4-2, and MCF-7 cells to express the FastFUCCI reporter which causes cells to fluoresce green, yellow, and orange during S/G2/M, G1/S, and G1, respectively (28), enabling quantitative image-based cell-cycle analysis (**Fig. 2A**). Using these reporter lines, we found no evidence that RBN-2397 altered the percentage of cells in each phase of the cell cycle (**Fig. 2B** and **C**; Supplementary Fig. S2A and S2B). However, when 22Rv1 and MCF-7 cells were treated with both tapinarof and RBN-2397, there was a decrease in the percentage of S/G2/M phases cells compared with RBN-2397 or tapinarof alone (**Fig. 2B**; Supplementary Fig. S2A). C4-2 cells treated with both RBN-2397 and tapinarof also showed an increase in G1/S cells and a concurrent decrease in S/G2/M cells. This shift occurred in an RBN-2397 concentration-dependent manner and was observed in cells treated for 24, 48, and 72 hours (**Fig. 2C**; Supplementary Fig. S2B). Consistent with a G1 arrest, 22Rv1 cells showed decreased levels of phosphorylated retinoblastoma protein (Rb) and C4-2 cells showed increased levels of p21 upon treatment with both RBN-2397 and tapinarof (**Fig. 2D**). No evidence of cleaved PARP1 was detected at these concentrations or time points (Supplementary Fig. S2C). Together these data support PARP7i and AHRa acting synergistically to arrest cells in G1.

To define the transcriptional effects of PARP7i and AHRa treatment, we performed RNA-seq on 22Rv1 cells treated for 48 hours with DMSO, 100 nmol/L RBN-2397, 100 nmol/L tapinarof, or 100 nmol/L RBN-2397 plus 100 nmol/L tapinarof (**Fig. 2E**). All drug treatments were performed in the presence of DHT which promotes growth of 22Rv1 cells. Principal component analysis showed segregation of the samples by treatment conditions (Supplementary Fig. S2D). In line with DHT promoting growth of 22Rv1 cells, GSEA revealed elevated expression of genes involved in DNA replication and the cell cycle in DHT-treated cells compared with vehicle-treated cells (Supplementary Fig. S2E). GSEA also revealed that RBN-2397 treatment caused decreased mRNA levels for genes associated with the "retinoblastoma gene in cancer" gene set (**Fig. 2F**). This effect was much stronger in cells treated with the combination of PARP7i and AHRa, which also showed lower levels of mRNAs associated with "retinoblastoma gene in cancer," "cell cycle," "DNA replication," and "DNA mismatch repair" compared with DMSO-treated cells (**Fig. 2G**). Transcriptional expression of genes in these pathways was also suppressed in cells treated with PARP7i and AHRa compared with either single agent (Supplementary Fig. S2E). These changes are consistent with the combined treatment inducing a G1 arrest. Of note, GSEA also showed that treatment with RBN-2397 and tapinarof promoted the "AHR pathway" and pathways that crosstalk with AHR transcriptional signaling, including "hypoxia-inducible factor-1α regulation," "vitamin D receptor," "nuclear receptor" subfamily, and "estrogen receptor pathway" (**Fig. 2G**). In this experiment, the levels of AHR target gene transcripts, including *PARP7*, *CYP1A1*, *CYP1A2*, and *CYP1B1*, were significantly higher in cells treated with PARP7i and AHRa than those dosed with either single agent (Supplementary Fig. S2F). Thus, the cell-cycle arrest phenotype induced by PARP7i and AHRa is accompanied by a decrease in mRNAs for genes involved in cell-cycle progression and an increase in AHR target gene transcripts.

Genetic inactivation of PARP7 synergizes with AHRa

PARP7 and the AHR encompass a feedback loop, with PARP7 repressing AHR activity via mono-ADP-ribosylation (6, 7) and the AHR promoting transcription of *PARP7* (29). To explore the role of PARP7 in the synergistic response, we used CRISPR/Cas9 to inactivate *PARP7* in two representative cell line models: MCF-7 (breast) and 22Rv1 (prostate; Supplementary Fig. S3A and S3B). In MCF-7 cells, genetic ablation of *PARP7* had a similar effect as RBN-2397 treatment on transcriptional activation of AHR target genes, with *PARP7* KO cells showing upregulation of *CYP1A1* and *CYP1B1* after treatment with either tapinarof or 10-CI-BBQ regardless of whether RBN-2397 was coadministered (**Fig. 3A**). *PARP7* KO cells (sgPARP7) were more sensitive to AHRa than parental control cells (nontargeting sgRNA), with PARP7 depletion and PARP7i causing similar shifts in AHRa sensitivity (**Fig. 3B** and **C**; Supplementary Fig. S3C and S3D).

We also tested the effect of ectopically expressing a Myc-tagged *PARP7* cDNA and found that although overexpression of PARP7 negatively impacted cell proliferation in MCF-7 and 22Rv1 cells (**Fig. 3D**; Supplementary S3E–S3G), it did not significantly shift the IC_{50} value of RBN-2397 alone or in combination with tapinarof (**Fig. 3E** and **F**). Induced expression of PARP7 sensitized PARP7 KO cells to both RBN-2397 alone and the combination of RBN-2397 and tapinarof (Supplementary Fig.

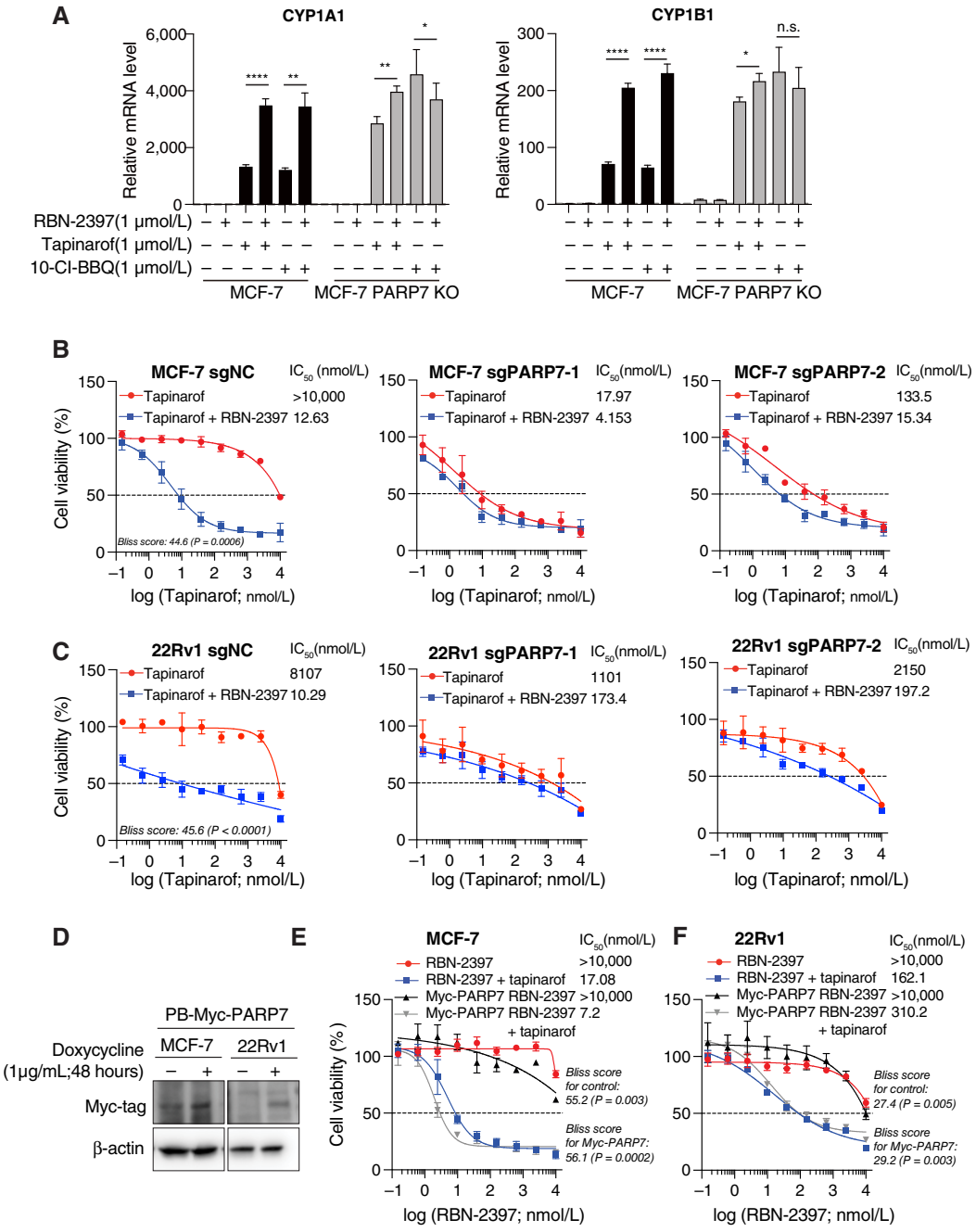

Figure 3.

PARP7 loss shows synergy with AHRa. **A,** RT-qPCR data showing relative mRNA levels of AHR transcriptional targets (*CYP1A1* and *CYP1B1*) in MCF-7 cells and *PARP7* KO cells treated with the indicated combinations of RBN-2397, tapinarof, and/or 10-Cl-BBQ for 24 hours. Data are shown as the mean ± SD; $n = 3$. Student *t* test was used to compare mRNA levels of each treatment. *, $P < 0.05$; **, $P < 0.01$; ***, $P < 0.001$; ****, $P < 0.0001$; **B,** Survival curves (IncuCyte) of parental and *PARP7* KO MCF-7 cells treated with increasing concentrations of tapinarof with or without fixed RBN-2397 (100 nmol/L) for 7 days. Data are shown as the mean ± SD; $n = 3$. **C,** Survival curves (CellTiter-Glo) of parental and *PARP7* KO 22Rv1 cells treated with increasing concentrations of tapinarof with or without fixed RBN-2397 (100 nmol/L) for 7 days. Data are shown as the mean ± SD; $n = 3$. **D,** Western blot analysis of lysates from MCF-7 and 22Rv1 parental cells and cells induced to express a Myc-tagged *PARP7* cDNA transgene. **E,** Survival curves (CellTiter-Glo) showing the effect of doxycycline-induced PARP7 overexpression in MCF-7 cells. Data are shown as the mean ± SD; $n = 3$. Bliss scores with *P* values are indicated. **F,** Survival curves (CellTiter-Glo) showing the effect of doxycycline-induced PARP7 overexpression in 22Rv1 cells. Data are shown as the mean ± SD; $n = 3$. Bliss scores with *P* values are indicated. n.s., not significant.

S3H). Together, the observations that RBN-2397 does not further increase synergy in *PARP7* KO cells and that RBN-2397 sensitivity can be restored by re-expressing PARP7 strongly support the conclusion that the synergistic drug response is mediated through the inhibition of PARP7 enzymatic activity by RBN-2397.

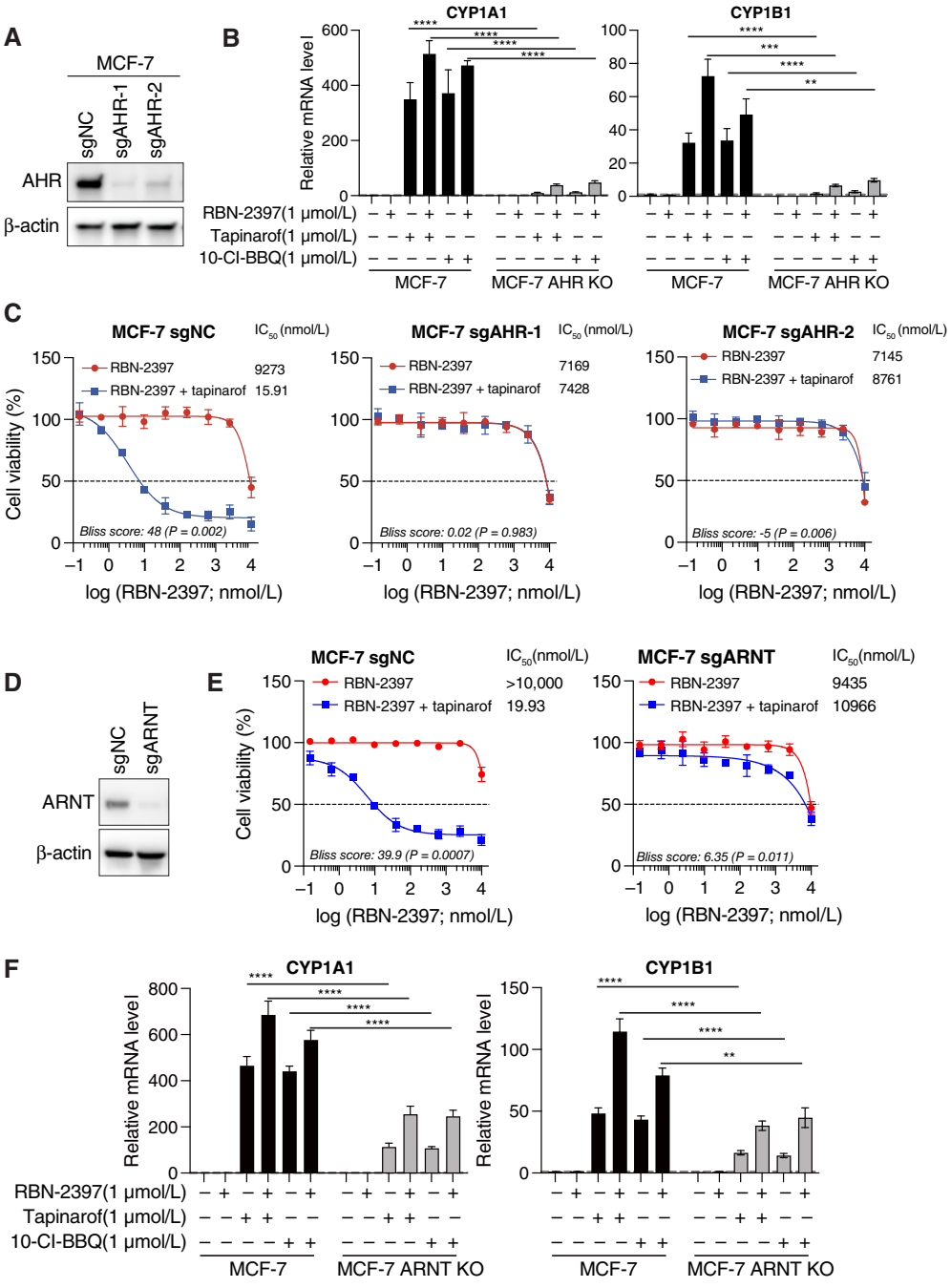

Figure 4.

AHR and ARNT required for the cellular response to AHRa and PARP7i. **A,** Western blot analysis of lysates from MCF-7 cells and *AHR* KO pools. **B,** RT-qPCR data showing relative mRNA levels of AHR transcriptional targets (*CYP1A1* and *CYP1B1*) in MCF-7 cells and *AHR* KO pools treated with the indicated combinations of RBN-2397, tapinarof, and/or 10-Cl-BBQ for 24 hours. Data are shown as the mean ± SD; $n = 3$. Student t test was used to compare mRNA levels of each treatment. *, $P < 0.05$; **, $P < 0.01$; ***, $P < 0.001$; ****, $P < 0.0001$. **C,** Survival curves (IncuCyte) of parental and *AHR* KO MCF-7 cells treated with increasing concentrations of RBN-2397 with or without fixed tapinarof (100 nmol/L) for 7 days. Data are shown as the mean ± SD; $n = 3$. Bliss scores with P values are indicated. **D,** Western blot analysis of lysates from MCF-7 cells and *ARNT* KO pools. **E,** Survival (IncuCyte) curves of parental and *ARNT* KO MCF-7 cells treated with increasing concentrations of RBN-2397 with or without fixed tapinarof (100 nmol/L) for 7 days. Data are shown as the mean ± SD; $n = 3$. Bliss scores with P values are indicated. **F,** RT-qPCR data showing relative mRNA levels of AHR transcriptional targets (*CYP1A1* and *CYP1B1*) in MCF-7 cells and *ARNT* KO pools treated with the indicated combinations of RBN-2397 and tapinarof or 10-Cl-BBQ for 24 hours. Data are shown as the mean ± SD; $n = 3$. Student t test was used to compare mRNA levels after each treatment. *, $P < 0.05$; **, $P < 0.01$; ***, $P < 0.001$; ****, $P < 0.0001$.

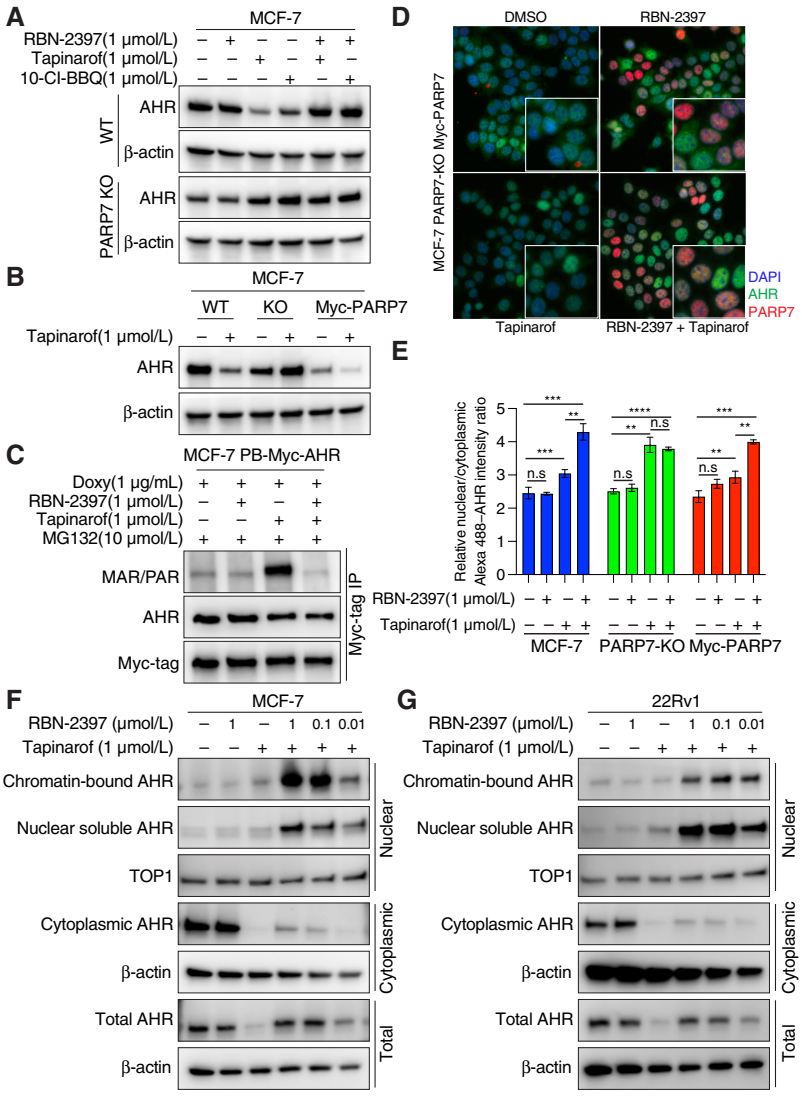

Figure 5.

Loss of PARP7 activity prevents AHRa-induced AHR degradation, causing increased nuclear AHR. **A,** Western blot analysis of lysates from MCF-7 and MCF-7 *PARP7* KO cells treated with the indicated combinations of RBN-2397 and tapinarof or 10-Cl-BBQ for 24 hours. **B,** Western blot analysis of lysates from MCF-7, MCF-7 *PARP7* KO, and MCF-7 *PARP7* KO cells overexpressing PARP7 treated with tapinarof for 24 hours. **C,** Western blot analysis of proteins that co-mmunoprecipitate with the AHR from MCF7 cells induced to express a Myc-tagged *AHR* transgene. Cells were treated with the indicated combinations of RBN-2397, MG132, and tapinarof for 3 hours. **D,** Representative immunofluorescence images of MCF-7 *PARP7* KO cells expressing a Myc-tagged *PARP7* transgene treated with RBN-2397, tapinarof, or a combination of both drugs for 4 hours. DMSO-treated cells are shown as a control. **E,** Relative ratio of nuclear/cytoplasmic AHR from **D**. Data are shown as the mean ± SD; >20,000 cells from triplicate wells were analyzed for each group. Student *t* test was used to compare mRNA levels of each treatment. *, $P < 0.05$; **, $P < 0.01$; ***, $P < 0.001$; ****, $P < 0.0001$. **F** and **G,** Western blot analysis of nuclear and cytoplasmic extracted lysates of (**F**) MCF-7 and (**G**) 22Rv1 cells treated with the indicated combinations of RBN-2397 and tapinarof for 4 hours. DAPI: 4′,6-diamidino-2-phenylindole; n.s., not significant.

The AHR and ARNT are required for the synergistic lethal effect of AHRa and PARP7i

To investigate the role of the AHR in the cellular response to PARP7i and AHRa, we used CRISPR/Cas9 to inactivate *AHR* in MCF-7 and 22Rv1 cells; loss of the AHR was confirmed by western blotting, and *AHR* KO cells showed a significant decrease in the mRNA levels of AHR transcriptional targets, including *CYPYA1* and *CYPYB1* (**Fig. 4A** and **B**; Supplementary Fig. S4A). Dose–response experiments in both 22Rv1 and MCF-7 *AHR* KO cells revealed that loss of the AHR abrogated the synergistic lethality of AHRa and PARP7i (**Fig. 4C**; Supplementary Fig. S4B and S4C), indicating that the AHR is critical for this effect. We also tested the effect of exogenous expression of the AHR and found that MCF-7 and 22Rv1 cells overexpressing the AHR showed enhanced synergy upon treatment with the combination of AHRa and PARP7i compared with parental control cells (Supplementary Fig. S4D and S4E).

Ligand-bound AHR forms a heterodimer with ARNT that binds to promoters of AHR target genes to promote transcription (30). Consistent with ARNT binding being necessary for AHR activity, the synergistic response to AHRa and PARP7i was abrogated in *ARNT* KO MCF-7 cells (**Fig. 4D** and **E**). ARNT-deficient cells also showed decreased transcriptional activation of the AHR targets *CYP1A1* and *CYP1B1* (**Fig. 4F**). Together, these results provide evidence that the synergistic cellular response to AHRa and PARP7i requires both AHR and ARNT. We note that although AHR is necessary for synergy, we find no correlation between response and AHR protein levels (Supplementary Fig. S4F), raising the possibility that induction of AHR activity, but not necessarily the amount of protein *per se*, drives the synergistic phenotype.

Loss of PARP7 activity blocks AHRa-induced AHR degradation and promotes increased levels of nuclear AHR

Concurrent with transcriptional activation of AHR target genes, the AHR is exported from the nucleus to the cytoplasm, where it is degraded via the proteasome (29). Nuclear export is necessary for AHR degradation, and PARP7 inhibition can promote nuclear retention of the AHR (22, 31). To understand how PARP7i and AHRa influence AHR turnover, we next measured the effect of these drugs, alone and

in combination, on AHR localization and protein levels. In agreement with previous reports, we found that MCF-7, 22Rv1, or LNCaP cells treated with AHRa had decreased steady-state AHR protein levels (**Fig. 5A**; Supplementary Fig. S5A). This decrease was not observed in MCF-7 *PARP7* KO or MCF-7 cells cotreated with PARP7i and AHRa, and PARP7i alone had no effect on AHR levels (**Fig. 5A**; Supplementary Fig. S5A). Conversely, we found that AHR protein levels were lower in cells engineered to overexpress PARP7 than in control cells (**Fig. 5B**). Thus, we conclude that the AHRa-induced decrease in AHR protein levels is dependent on PARP7 enzymatic activity. PARP7 likely regulates AHR levels through a post-transcriptional mechanism as PARP7i did not affect the levels of *AHR* mRNA (Supplementary Fig. S5B).

PARP7 has been shown to ADP-ribosylate (ADPr) the AHR (5, 6), so we next performed immunoprecipitation experiments to measure ADPr modification of the AHR after drug treatment. In addition to RBN-2397 and tapinarof, cells were also treated with the proteasomal inhibitor MG132 to block proteasomal turnover of the AHR (Supplementary Fig. S5C). Our data confirm that PARP7i blocks AHRa-induced MAR/PARylation of the AHR (**Fig. 5C**), in line with PARP7 regulating AHR protein levels through ADP-ribosylation (6, 7). We considered the possibility that PARP7-mediated ADP-ribosylation of the AHR may also influence AHR ubiquitination, however, AHR pulldown experiments showed similar levels of ubiquitinated protein across all treatment conditions (Supplementary Fig. S5D). MCF-7 cells treated with both PARP7i and AHRa did, however, show a significant increase in the nuclear/cytoplasmic ratio of the AHR. In MCF-7 *PARP7* KO cells, AHRa alone causes an increase in the nuclear/cytoplasmic ratio of AHR, whereas the addition of RBN-2397 showed no additional increase. Notably, overexpression of PARP7 in *PARP7* KO cells reversed this increase (**Fig. 5D** and **E**), consistent with PARP7-mediated ADPr regulating the subcellular localization of the AHR (6, 7). Because it is challenging to accurately quantify the distribution of nuclear and cytoplasmic AHR by immunofluorescence, we used nuclear/cytoplasmic fractionation to monitor AHR protein localization by western blotting. Although RBN-2397 alone had no effect on AHR levels or distribution, MCF-7 and 22Rv1 cells treated with tapinarof showed decreased levels of cytoplasmic AHR. In contrast, cells treated with both RBN-2397 and tapinarof showed increased levels of nuclear soluble AHR and chromatin-bound AHR (**Fig. 5F** and **G**). Overall, the increase in total nuclear AHR levels in both cell lines was positively correlated with the dose of RBN-2397. Consistent with PARP7i phenocopying PARP7 loss, MCF-7 *PARP7* KO cells showed increased nuclear and chromatin-bound AHR upon treatment with tapinarof, but the addition of RBN-2397 caused no additional increase (Supplementary Fig. S5E). We conclude that PARP7 regulates the cellular distribution of the AHR and likely blocks transcription of AHR targets by reducing levels of active nuclear/chromatin-bound AHR.

PARP7i and AHRa synergistically suppress the *in vitro* growth of hormone-resistant cancer cell lines and promote proteasomal turnover of hormone receptors

We noted that some of the cell lines that responded synergistically to pharmacologic inhibition of PARP7 and AHRa were hormone-regulated, including ERα-positive MCF-7 breast cancer cells and PEO1 and PEO4 ovarian cancer cells and the AR-positive prostate cancer cells, 22Rv1 and LNCaP (**Fig. 1A** and **B**). The ER and AR are both substrates of PARP7 (32, 33) and it has been shown previously that PARP7 and AHR can modulate both estrogen and androgen signaling (19, 33). To further investigate the relationship between steroid hormone receptors (HR) and PARP7i/AHRa response, we performed western blot analysis to measure the effect of these drugs, alone and in combination, on steady-state levels of ERα and AR proteins. Although RBN-2397 alone had no effect on ERα levels, MCF-7 cells treated with tapinarof showed decreased steady-state levels of ERα. After 6 hours, MCF-7 cells treated with the combination of AHRa and PARP7i showed an initial increase in ERα levels; however, by 48 hours, cells treated with both drugs showed a complete loss of ERα protein (**Fig. 6A**). Parallel experiments in the AR-positive prostate cancer cell line 22Rv1 revealed a similar effect, with tapinarof alone inducing a decrease in AR protein levels, whereas cells treated with both tapinarof and RBN-2397 showed an initial spike in AR expression after 6 hours, followed by a complete loss of AR protein at 72 hours (**Fig. 6B**). No change in ERα or AR levels was observed at any time points in cells treated with RBN-2397 alone (**Fig. 6A** and **B**). Together, these data suggest that adding RBN-2397 to AHRa treatment can enhance AHR-mediated turnover of HRs at later time points.

In addition to the full-length AR (AR-FL), 22Rv1 cells also express an AR splice variant, AR-v7, that is associated with hormone therapy resistance (34–36). We noted that the level of AR-FL and AR-v7 proteins were both reduced in 22Rv1 cells treated with PARP7i and AHRa (**Fig. 6B**), indicating that both isoforms were subject to AHR-mediated turnover. As AR-v7 is associated with resistance to antiandrogen agents, we next used siRNA to knock down AR-FL to measure the effect of AHRa and PARP7i on cells only expressing hormone-resistant AR-v7 (Supplementary Fig. S6A). Notably, cells expressing only AR-v7 and not AR-FL remained sensitive to the combination of RBN-2397 and tapinarof (Supplementary Fig. S6B), suggesting the possibility that dual targeting of AHR and PARP7 may be a novel therapeutic strategy to overcome hormone therapy resistance mediated by AR-v7.

To further test this hypothesis, we measured how MCF-7 cells engineered to carry ET-resistant *ESR1*-mutant alleles responded to AHRa and PARP7i treatment. *ESR1* Y537S, *ESR1* Y537C, and *ESR1* D538G mutant MCF-7 cell lines were generated by CRISPR-mediated knock-in and confirmed by sequencing (Supplementary Fig. S6C). Although all three mutant cell lines were resistant to fulvestrant (**Fig. 6C**), they all showed a synergistic response to tapinarof and RBN-2937 (**Fig. 6D**), similar to WT MCF-7 cells (**Fig. 1A**). Because the D538G mutant cell line is heterozygous and also expresses WT ER (Supplementary Fig. S6C), we also tested how all three *ESR1*-mutant lines responded to tapinarof and RBN-2397 in charcoal-stripped serum-containing phenol red–free media (CSS media). In these conditions, all three lines still showed synergy, confirming the inhibitory effect of the drug combination on *ESR1*-mutant–driven growth (Supplementary Fig. S6D). Consistent with results for other cells that exhibited synergy, both inhibition and KO of *PARP7* in *ESR1* Y537S mutant MCF-7 cells combined with tapinarof inhibited cell growth, and loss of AHR in *ESR1* Y537S mutant cells abrogated the synergistic effect of RBN-2397 and tapinarof (Supplementary Fig. S6E–S6G). MCF-7 *ESR1* Y537S mutant cells treated with the combination of PARP7i and AHRa had a reduced percent of cells in S/G2/M cells compared with either single agent alone (**Fig. 6E**). Notably, unlike fulvestrant, which only affected ERα protein levels in parental but not *ESR1*-mutant MCF-7 cells (**Fig. 6F**), western blot analysis showed reduced levels of Y537S ERα in cells treated with tapinarof and a complete loss of the mutant protein at 72 hours in cells treated with both drugs (**Fig. 6G**). Acquired *HER2* mutations in ERα+ metastatic breast cancer are also reported to confer resistance to hormone therapies (37), so we next tested synergy in a *HER2* mutation–driven MCF-7 cell line model and found that the combination of AHRa and PARP7i also inhibited the growth of these cells (Bliss scores > 10), providing further evidence that this combination can control growth of hormone-refractory tumors (**Fig. 6H**).

Ligand-bound AHR can form a ubiquitin ligase complex with CUL4B which has been implicated in proteolysis of AR and ERα (38),

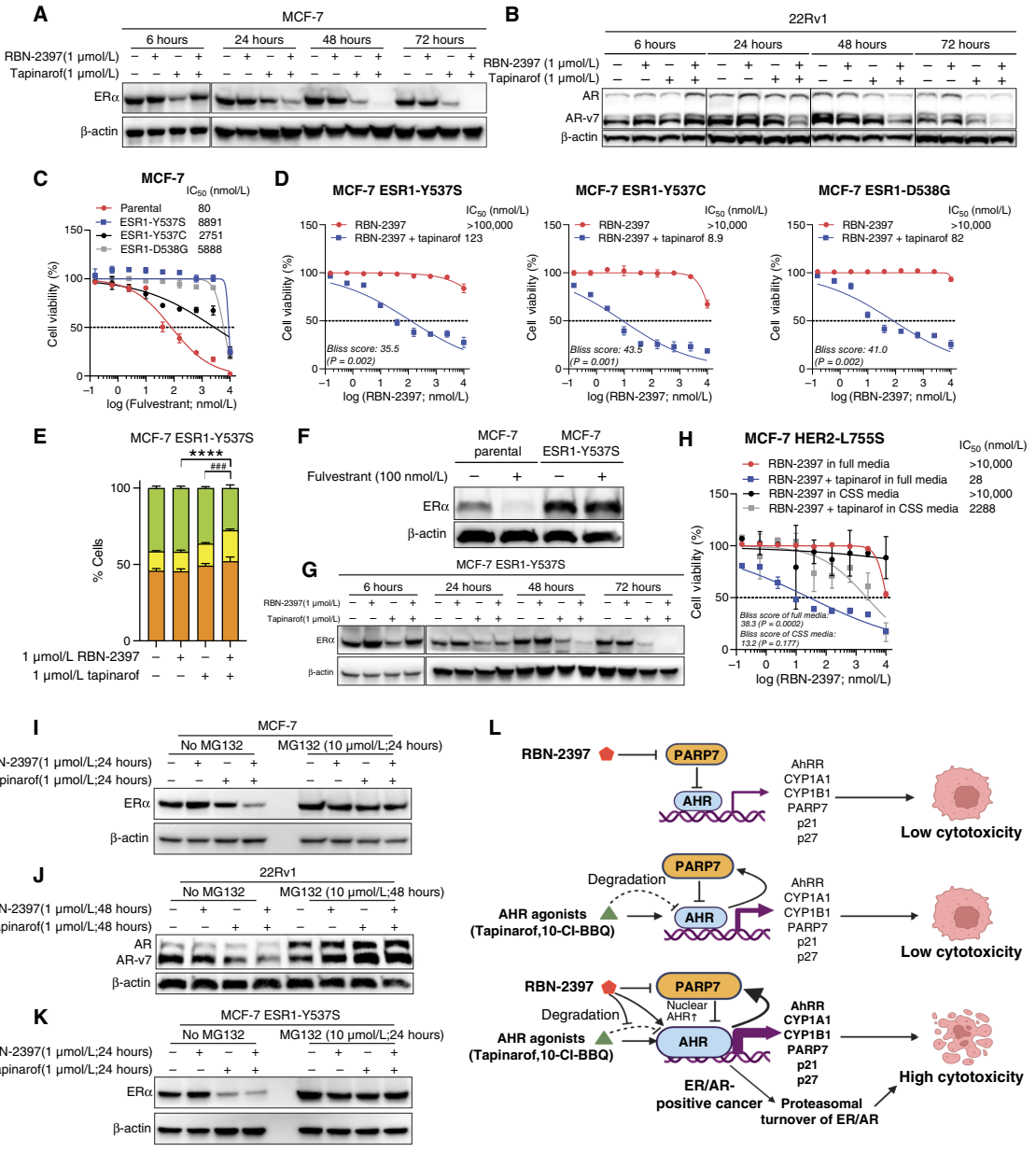

Figure 6.

PARP7i and AHRa synergistically suppress the *in vitro* growth of hormone-resistant cancer cell lines. **A** and **B,** Western blot analysis of lysates from (**A)** MCF-7 cells and (**B)** 22Rv1 cells treated with the indicated combinations of RBN-2397 and/or tapinarof for 6, 24, 48, or 72 hours. **C,** Survival curves (IncuCyte) of parental MCF-7 cells and *ESR1* Y537S, *ESR1* Y537C, or *ESR1* D538G MCF-7 cells treated with increasing concentration of fulvestrant. Data are shown as the mean ± SD; $n = 3$. **D,** Survival curves (IncuCyte) of MCF-7 cells expressing *ESR1* Y537S, *ESR1* Y537C, or *ESR1* D538G treated with increasing concentrations of RBN-2397 with/without fixed tapinarof (100 nmol/L). Data are shown as the mean ± SD; $n = 3$. Bliss scores with *P* values are indicated. **E,** Plots showing the percent of MCF-7 *ESR1* Y537S cells expressing the FastFUCCI reporter in each phase of the cell cycle after 72 hours of treatment with indicated concentrations of RBN-2397 and tapinarof. Green, yellow, and orange correspond to cells in S/G2/M, G1/S, and G1, respectively. One-way ANOVA followed by Tukey multiple comparisons test was used to compare S/G2/M cells of each treatment. */#, $P < 0.05$; **/##, $P < 0.01$; ***/###, $P < 0.001$; ****/####, $P < 0.0001$. **F,** Western blot analysis of lysates from parental and *ESR1* Y537S MCF-7 cells treated with the indicated concentrations of fulvestrant. **G,** Western blot analysis of lysates from *ESR1* Y537S MCF-7 cells treated with the indicated combinations of RBN-2397 and/or tapinarof for 6, 24, 48, or 72 hours. **H,** Survival curves (IncuCyte) of *HER2* L755S MCF-7 cells treated with RBN-2397 with or without a fixed concentration of tapinarof (100 nmol/L) in complete or CSS media. Data are shown as the mean ± SD; $n = 3$. Bliss scores with *P* values are indicated. **I–K,** Western blot analysis of lysates from (**I)** MCF-7, (**J**) 22Rv1, or (**K**) *ESR1* Y537S MCF-7 cells treated with the indicated combinations of RBN-2397, tapinarof and MG132 for 24 hours. **L,** Proposed model for synergistic lethal effect of PARP7i and AHRa. Top, Single-agent PARP7i causes a slight increase in AHR activity, with low cytotoxicity. Middle, Single-agent AHRa promotes degradation of the AHR and activates transcription of AHR target genes, including PARP7, attenuating AHR activity. This negative feedback loop prevents excessive AHR activation and cytotoxicity. Bottom, In cells treated with PARP7i and AHRa, AHRa activates the AHR, whereas PARP7i promotes AHR nuclear retention, resulting in constitutive AHR activity and cytotoxicity. In ER/AR-positive cells, constitutively active AHR also promotes turnover of steroid HRs and negatively impacts cell proliferation. (Created with BioRender.com.)

and, therefore, the increase in nuclear AHR in cells treated with PARP7i and AHRa might promote proteasomal turnover of HRs. To test this hypothesis, we used MG132 to inhibit proteasomal proteolytic activity and found that this treatment restored ERα and AR protein levels in MCF-7 and 22Rv1 cells treated with tapinarof and RBN-2397 (**Fig. 6I** and **J**). ERα levels were also restored in MCF-7 *ESR1* Y537S cells treated with MG132 (**Fig. 6K**). We note that ERα levels were unaffected by AHRa and PARP7i in *ARNT* KO cells, suggesting that AHR/ARNT is required for this process (Supplementary Fig. S6H and S6I). Together, these results show that PARP7i and AHRa work synergistically to drive proteasomal turnover of both WT and mutant HRs, providing evidence that this combination of drugs could be used to treat hormone-refractory tumors.

Discussion

Accumulating evidence suggests that inhibition of the mono (ADP) ribosyl transferase PARP7 may be a novel and useful approach to treat various cancers, and multiple PARP7i are being investigated in preclinical and clinical studies (19, 20, 39, 40); NCT04053673 and NCT05127590). We previously reported that AHRa can enhance the effect of PARP7i in tumor cell lines showing intrinsic sensitivity to PARP7i (22). In this study, we investigated the therapeutic effect of combining PARP7i and AHRa across a broad panel of cell line models. Unexpectedly, we found that for the preponderance of the cancer cell lines tested, cell growth was synergistically suppressed by the combination of the two agents, whereas each agent alone had only modest effects. It is important to note that several cancer cell lines failed to show a synergistic response to PARP7i and AHRa. In addition, the combination did not inhibit the growth of untransformed epithelial cells (HEK293T and MCF10A) and primary $CD8^+$ T cells, suggesting that this is not a pan-lethal effect.

PARP7 acts to repress AHR transactivation, and inhibition of PARP7 by RBN-2397 can block PARP7-mediated ADP-ribosylation of the AHR, causing elevated transcription of AHR target genes (**Figs. 3A** and **6L;** refs. 6, 41). When used alone, AHRa also induce an increase in transcription of AHR targets, including PARP7 and AHRR, but this increase rapidly causes the AHR to be exported from the nucleus and degraded, forming a negative feedback loop in which PARP7 attenuates sustained AHR activation (**Figs. 5** and **6L**; refs. 6, 22). In both conditions, AHR activation is controlled and does not lead to cellular cytotoxicity. However, when AHRa and PARP7i are used in combination, the AHRa promotes nuclear localization and transcriptional activation of the AHR and the PARP7i prevents PARP7 from deactivating the AHR. Therefore, the levels of nuclear AHR remain high, and we propose that this constitutive activation of AHR transcriptional programs leads to cytotoxicity (**Fig. 6L**).

Constitutively active AHR has been shown to interact with HRs and may play a role in the progression of hormone-related cancers (33, 42). In the current study, we find that sustained activation of the AHR in cells treated with both PARP7i and AHRa is associated with proteasomal turnover of the steroid HRs ERα and AR and cell-cycle arrest (**Figs. 2** and **6**). This result builds on previous reports that the ligand-bound AHR can form an atypical E3-ligase complex with CUL4B that promotes turnover of ERα and AR (34, 37) and that AHRa treatment causes a decrease in ERα and AR levels (38). Interestingly, we find that the addition of a PARP7i enhances this effect, resulting in a sustained loss of ERα and AR proteins. As PARP7 can negatively regulate the ERα and AR via mono-ADP-ribosylation in human breast cancer cells (31–33, 42), it is tempting to speculate that AHR and PARP7 work synergistically to regulate proteasomal turnover of HRs through multiple parallel pathways. In addition to promoting turnover of WT receptors, we show that sustained activation of the AHR is also associated with reduced levels of mutated ERα protein and AR-v7, a constitutively active splice variant of the AR. This finding may have significant implications as it suggests that combining AHRa and PARP7i may be a novel strategy to treat HR-driven tumors that are refractory to ET.

Although our data provide evidence that combining PARP7i with AHRa may extend the utility of these drugs to a wider range of tumors, including HR-driven tumors, more work is needed before these results can be translated clinically. One outstanding question is which AHRa might be most suitable for this application. Currently, tapinarof is the only AHRa approved by the FDA, and it is used as a topical agent to treat plaque psoriasis [reviewed in ref. 43]. In addition to tapinarof, we also tested two other agonists in this study: 10-Cl-BBQ and FICZ. Although both of these agents also showed synergy with RBN-2397, their pharmacologic properties may limit clinical use. Moreover, differences in the potency and half-life in the circulation of AHRa may affect the duration and level of AHR stimulation and, therefore, the effects of combining AHRa and PARP7i. Dosing and scheduling of the combination will need careful consideration to optimize efficacy and minimize potential toxicity. In summary, we show that AHRa can enhance PARP7i response across numerous cancer cell line models, but some models and untransformed cells do not show a synergistic response, suggesting there may be a therapeutic window for the combination. Further experiments to better understand the determinants of sensitivity and to define predictive signatures of response will, therefore, be important in utilizing this combination therapeutically.

Authors' Disclosures

A. Ashworth reports grants from Benioff Initiative in Prostate Cancer Research, V foundation, Gray Foundation, and the Breast Cancer Research Foundation (BCRF) during the conduct of the study and personal fees from Tango Therapeutics, Azkarra Therapeutics, Kytarro, Cytomx, Ovibio Corporation, Cambridge Science Corporation, Genentech, GLAdiator, Circle, Bluestar/Clearnote Health, Earli, Ambagon, Phoenix Molecular Designs, Yingli/280Bio, Trial Library, ORIC, HAP10, ProLynx, Next RNA, and Novartis and grants from Sun Pharma Advanced Research Company (SPARC) outside the submitted work; in addition, he holds patents on the use of PARP inhibitors held jointly with AstraZeneca from which he has benefited financially (and may do so in the future). No disclosures were reported by the other authors.

Authors' Contributions

H. Chen: Conceptualization, data curation, formal analysis, validation, investigation, visualization, methodology, writing–original draft, writing–review and editing. **X. Gou:** Conceptualization, data curation, formal analysis, validation, investigation, visualization, methodology, writing–original draft, writing–review and editing. **Y. Mao:** Data curation, validation, investigation. **P.C. O'Leary:** Data curation, validation, investigation. **M.E. Diolaiti:** Formal analysis, supervision, methodology, writing–original draft, project administration, writing–review and editing. **A. Ashworth:** Conceptualization, resources, supervision, funding acquisition, writing–original draft, project administration, writing–review and editing.

Acknowledgments

This research was supported by the University of California San Francisco (UCSF) Benioff Initiative for Prostate Cancer Research and the Breast Cancer Research Foundation, the V Foundation for Cancer Research and the Gray Foundation. Additional funding was received from The Susan G. Komen Breast Cancer Foundation, the NIH U54 CA209891, and Emerson Collective.

Note

Supplementary data for this article are available at Molecular Cancer Therapeutics Online (http://mct.aacrjournals.org/).

Received March 22, 2024; revised June 13, 2024; accepted September 11, 2024; published first September 23, 2024.

References

1. Nebert DW. Aryl hydrocarbon receptor (AHR): "pioneer member" of the basic-helix/loop/helix per-Arnt-sim (bHLH/PAS) family of "sensors" of foreign and endogenous signals. Prog Lipid Res 2017;67:38–57.
2. Opitz CA, Litzenburger UM, Sahm F, Ott M, Tritschler I, Trump S, et al. An endogenous tumour-promoting ligand of the human aryl hydrocarbon receptor. Nature 2011;478:197–203.
3. Bessede A, Gargaro M, Pallotta MT, Matino D, Servillo G, Brunacci C, et al. Aryl hydrocarbon receptor control of a disease tolerance defence pathway. Nature 2014;511:184–90.
4. Yamamoto T, Hatabayashi K, Arita M, Yajima N, Takenaka C, Suzuki T, et al. Kynurenine signaling through the aryl hydrocarbon receptor maintains the undifferentiated state of human embryonic stem cells. Sci Signal 2019;12: eaaw3306.
5. Gomez A, Bindesbøll C, Satheesh SV, Grimaldi G, Hutin D, MacPherson L, et al. Characterization of TCDD-inducible poly-ADP-ribose polymerase (TIPARP/ARTD14) catalytic activity. Biochem J 2018;475:3827–46.
6. MacPherson L, Tamblyn L, Rajendra S, Bralha F, McPherson JP, Matthews J. 2,3,7,8-Tetrachlorodibenzo-p-dioxin poly(ADP-ribose) polymerase (TiPARP, ARTD14) is a mono-ADP-ribosyltransferase and repressor of aryl hydrocarbon receptor transactivation. Nucleic Acids Res 2013;41:1604–21.
7. Rijo MP, Diani-Moore S, Yang C, Zhou P, Rifkind AB. Roles of the ubiquitin ligase CUL4B and ADP-ribosyltransferase TiPARP in TCDD-induced nuclear export and proteasomal degradation of the transcription factor AHR. J Biol Chem 2021;297:100886.
8. Ohtake F, Fujii-Kuriyama Y, Kato S. AhR acts as an E3 ubiquitin ligase to modulate steroid receptor functions. Biochem Pharmacol 2009;77:474–84.
9. Osborne CK, Schiff R. Mechanisms of endocrine resistance in breast cancer. Annu Rev Med 2011;62:233–47.
10. Osborne CK, Wakeling A, Nicholson RI. Fulvestrant: an oestrogen receptor antagonist with a novel mechanism of action. Br J Cancer 2004;90(Suppl 1): S2–6.
11. Merenbakh-Lamin K, Ben-Baruch N, Yeheskel A, Dvir A, Soussan-Gutman L, Jeselsohn R, et al. D538G mutation in estrogen receptor-α: a novel mechanism for acquired endocrine resistance in breast cancer. Cancer Res 2013;73:6856–64.
12. Robinson DR, Wu Y-M, Vats P, Su F, Lonigro RJ, Cao X, et al. Activating ESR1 mutations in hormone-resistant metastatic breast cancer. Nat Genet 2013;45:1446–51.
13. Toy W, Shen Y, Won H, Green B, Sakr RA, Will M, et al. ESR1 ligand-binding domain mutations in hormone-resistant breast cancer. Nat Genet 2013;45: 1439–45.
14. Gou X, Anurag M, Lei JT, Kim B-J, Singh P, Seker S, et al. Transcriptional reprogramming differentiates active from inactive ESR1 fusions in endocrine therapy-refractory metastatic breast cancer. Cancer Res 2021;81:6259–72.
15. Attard G, Parker C, Eeles RA, Schröder F, Tomlins SA, Tannock I, et al. Prostate cancer. Lancet 2016;387:70–82.
16. Gillessen S, Omlin A, Attard G, de Bono JS, Efstathiou E, Fizazi K, et al. Management of patients with advanced prostate cancer: recommendations of the St Gallen Advanced Prostate Cancer Consensus Conference (APCCC) 2015. Ann Oncol 2015;26:1589–604.
17. Cheng L, Li Z, Huang Y-Z, Zhang X, Dai X-Y, Shi L, et al. TCDD-inducible poly-ADP-ribose polymerase (TIPARP), A novel therapeutic target of breast cancer. Cancer Manag Res 2019;11:8991–9004.
18. Gozgit JM, Vasbinder MM, Abo RP, Kunii K, Kuplast-Barr KG, Gui B, et al. PARP7 negatively regulates the type I interferon response in cancer cells and its inhibition triggers antitumor immunity. Cancer Cell 2021;39:1214–26.e10.
19. Gu H, Yan W, Wang Y, Xu W, Huang L, Yang J, et al. Discovery of the potent and highly selective PARP7 inhibitor as a novel immunotherapeutic agent for tumors. J Med Chem 2023;66:473–90.
20. Sanderson DJ, Rodriguez KM, Bejan DS, Olafsen NE, Bohn ID, Kojic A, et al. Structurally distinct PARP7 inhibitors provide new insights into the function of PARP7 in regulating nucleic acid-sensing and IFN-beta signaling. Cell Chem Biol 2023;30:43–54 e8.
21. Rasmussen M, Alvik K, Kannen V, Olafsen NE, Erlingsson LAM, Grimaldi G, et al. Loss of PARP7 increases type I interferon signaling in EO771 breast cancer cells and prevents mammary tumor growth by increasing antitumor immunity. Cancers (Basel) 2023;15:3689.
22. Chen H, Diolaiti ME, O'Leary PC, Rojc A, Krogan NJ, Kim M, et al. A whole-genome CRISPR screen identifies AHR loss as a mechanism of resistance to a PARP7 inhibitor. Mol Cancer Ther 2022;21:1076–89.
23. Langmead B, Salzberg SL. Fast gapped-read alignment with Bowtie 2. Nat Methods 2012;9:357–9.
24. Li B, Dewey CN. RSEM: accurate transcript quantification from RNA-Seq data with or without a reference genome. BMC Bioinformatics 2011;12:323.
25. Liao Y, Wang J, Jaehnig EJ, Shi Z, Zhang B. WebGestalt 2019: gene set analysis toolkit with revamped UIs and APIs. Nucleic Acids Res 2019;47:W199–205.
26. Shifrut E, Carnevale J, Tobin V, Roth TL, Woo JM, Bui CT, et al. Genome-wide CRISPR screens in primary human T cells reveal key regulators of immune function. Cell 2018;175:1958–71.e15.
27. Zheng S, Wang W, Aldahdooh J, Malyutina A, Shadbahr T, Tanoli Z, et al. SynergyFinder plus: toward better interpretation and annotation of drug combination screening datasets. Genomics Proteomics Bioinformatics 2022; 20:587–96.
28. Koh S-B, Mascalchi P, Rodriguez E, Lin Y, Jodrell DI, Richards FM, et al. A quantitative FastFUCCI assay defines cell cycle dynamics at a single-cell level. J Cell Sci 2017;130:512–20.
29. Ma Q, Baldwin KT. 2,3,7,8-tetrachlorodibenzo-p-dioxin-induced degradation of aryl hydrocarbon receptor (AhR) by the ubiquitin-proteasome pathway. Role of the transcription activaton and DNA binding of AhR. J Biol Chem 2000;275:8432–8.
30. Beischlag TV, Luis Morales J, Hollingshead BD, Perdew GH. The aryl hydrocarbon receptor complex and the control of gene expression. Crit Rev Eukaryot Gene Expr 2008;18:207–50.
31. Yang C, Wierbiłowicz K, Dworak NM, Bae SY, Tengse SB, Abianeh N, et al. Induction of PARP7 creates a vulnerability for growth inhibition by RBN2397 in prostate cancer cells. Cancer Res Commun 2023;3:592–606.
32. Yang C-S, Jividen K, Kamata T, Dworak N, Oostdyk L, Remlein B, et al. Androgen signaling uses a writer and a reader of ADP-ribosylation to regulate protein complex assembly. Nat Commun 2021;12:2705.
33. Rasmussen M, Tan S, Somisetty VS, Hutin D, Olafsen NE, Moen A, et al. PARP7 and mono-ADP-ribosylation negatively regulate estrogen receptor alpha signaling in human breast cancer cells. Cells 2021;10:623.
34. Wadosky KM, Koochekpour S. Androgen receptor splice variants and prostate cancer: from bench to bedside. Oncotarget 2017;8:18550–76.
35. Antonarakis ES, Lu C, Wang H, Luber B, Nakazawa M, Roeser JC, et al. AR-V7 and resistance to enzalutamide and abiraterone in prostate cancer. N Engl J Med 2014;371:1028–38.
36. Antonarakis ES, Lu C, Luber B, Wang H, Chen Y, Zhu Y, et al. Clinical significance of androgen receptor splice variant-7 mRNA detection in circulating tumor cells of men with metastatic castration-resistant prostate cancer treated with first- and second-line abiraterone and enzalutamide. J Clin Oncol 2017;35:2149–56.
37. Nayar U, Cohen O, Kapstad C, Cuoco MS, Waks AG, Wander SA, et al. Acquired HER2 mutations in ER^+ metastatic breast cancer confer resistance to estrogen receptor-directed therapies. Nat Genet 2019;51:207–16.
38. Ohtake F, Baba A, Takada I, Okada M, Iwasaki K, Miki H, et al. Dioxin receptor is a ligand-dependent E3 ubiquitin ligase. Nature 2007;446:562–6.
39. Xu J, Zhao A, Chen D, Wang J, Ma J, Qing L, et al. Discovery of tricyclic PARP7 inhibitors with high potency, selectivity, and oral bioavailability. Eur J Med Chem 2024;266:116160.
40. Gu H, Yan W, Yang J, Liu B, Zhao X, Wang H, et al. Discovery of highly selective PARP7 inhibitors with a novel scaffold for cancer immunotherapy. J Med Chem 2024;67:1932–48.
41. Ahmed S, Bott D, Gomez A, Tamblyn L, Rasheed A, Cho T, et al. Loss of the mono-ADP-ribosyltransferase, tiparp, increases sensitivity to dioxin-induced steatohepatitis and lethality. J Biol Chem 2015;290:16824–40.
42. Kamata T, Yang C-S, Paschal BM. PARP7 mono-ADP-ribosylates the agonist conformation of the androgen receptor in the nucleus. Biochem J 2021;478: 2999–3014.
43. Keam SJ. Tapinarof cream 1%: first approval. Drugs 2022;82:1221–8.